Sub-100 nanometer transverse gratings written by femtosecond laser pulses on a titanium surface

Andrey A Ionin[1], Sergey I Kudryashov[1], Sergey V Makarov[1], Leonid V Seleznev[1], Dmitry V Sinitsyn[1], Alexander E Ligachev[2], Evgene V Golosov[3,4] and Yury R Kolobov[3,4]

[1] P N Lebedev Physical Institute RAS, Leninskiy prospect 53, 119991 Moscow, Russia
[2] A M Prokhorov General Physics Institute RAS, Vavilova street 38, 119991 Moscow, Russia
[3] Belgorod State University, Pobedy Street 85, 308015 Belgorod, Russia
[4] Institute of Structural Macrokinetics and Materials Science RAS, Academician Osipyan str. 8, 142432 Chernogolovka, Moscow Region, Russia

E-mail: sikudr@lebedev.ru

Abstract

One-dimensional transverse (perpendicular to the laser polarization) gratings with periods $\Lambda \approx 50$–60 nm were observed on a titanium surface within 150 nm wide, micrometer-long regular surface modification longitudinal stripes fabricated by multiple 744 nm Ti:sapphire femtosecond laser shots, occurring at a repetition rate of 10 Hz. In the center of the surface laser spot these stripes are oriented strictly perpendicular to the laser polarization, in accordance with the plasmon-polaritonic model, and appear as ablative longitudinal trenches centered along the main stripe axes, which are precursors of longitudinal common ripples with a 500 nm period. At the low-fluence periphery of the laser spot, the stripes appear not as ablative longitudinal trenches, but as linear arrays of sub-ablative *transverse* nanoripples with periods down to 50 nm. The appearance of such superfine transverse nanoripples is related to incomplete spallation of the laser–molten surface layer, periodically modulated at the nanoscale through coherent sub-surface cavitation.

1. Introduction

Short-pulse (femtosecond/fs and short picosecond) lasers provide a unique opportunity for large-scale parallel fabrication of one- or two-dimensional quasi-regular arrays of nanoscale surface structures (sub-micron ripples [1–3] or spikes [4, 5]), exhibiting in such grand ensembles unusual physical and physico-chemical properties, e.g. optical [6, 7] and wetting [8, 9] properties. Typically, such quasi-regular sub-micron arrays exhibit spatial periods close to the pump laser wavelength λ, due to constructive interference between the incident laser wave and its interface (surface plasmon-polariton, SPP) counterpart, excited via scattering of the former wave on the initial seeding surface roughness [10–13]. At the normal incidence of the exciting laser wave, the maximum growth rate of the ripple amplitude is achieved for ripples with wavevectors collinear to the laser polarization, since at this orientation both Stokes and anti-Stokes SPPs give equal contributions to the ripple generation [11]. Since the SPP wavelength Λ_{SPP} is determined by an angle of laser incidence, optical constants of the boundary media and the laser wavelength [10–13], the approximate equity (within the factor $\lambda/\Lambda_{SPP} \approx 1$–1.5) of the laser and SPP wavelengths at the air–metal interface can be tuned toward $\Lambda_{SPP} < \lambda$ in some limited range either via laser variation of their optical constants [14–16], or choice of the top

transparent medium with higher refractive index [5, 15, 16], or near-threshold surface nanostructuring providing not a single, but a whole set of higher surface relief harmonics with spatial periods Λ_{nano}/m [16, 17], where m is an integer number. Furthermore, the strong, almost proportional decrease in Λ can be achieved by spectral tuning the laser wavelength λ to the UV region, though in this case variation of λ will be limited at 200–250 nm, the blue edge of transmission for air and other typical transparent media [16]. Overall, the current advances in laser surface nanostructuring, using this common 'laser–SPP interference' approach, are limited by minimal periods of 60–80 nm for multiple surface gratings (i.e. unharmonic nanoripples, containing multiple spatial harmonics, in the form of relief beatings) [16], 120 nm minimal periods for nanospike arrays fabricated in water [5] or 190 nm periods for nanoripples produced by a UV fs-laser [16]. Hence, new approaches in laser nanostructuring of surfaces are demanding the fabrication of truly nanoscale feature arrays with single periods in the sub-100 nm range, where principal nanoscale effects become pronounced.

Recently, irregular [18–20] and regular [21] sets of sub-micron (~200 nm) surface spikes were experimentally observed on various dielectric and metallic surfaces, respectively, indicating that new, unexplored surface nanostructuring mechanisms (e.g. Coulomb explosion, field ion emission or thermal ablation [19]) may become operative at more mild laser irradiation conditions (lower doses). Meanwhile, based on previous molecular dynamics (MD) simulations [22] and direct experimental observations of separate spalled spike caps [21], these un-organized and self-organized surface sub-micron structures were related, respectively, to incoherent [22] and coherent [21] nanoscale cavitation in the thin surface molten layers, resulting in incomplete ('frozen') spallation of the sub-surface nanobubble caps (for important recent findings on the spallation mechanism see [23]) at spallation sub-threshold fluences [21]. However, despite emerging technological perspectives of the parallel low-fluence deep-subwavelength surface structuring regime, the basic relationships between laser, material and nanofeature parameters, as well as up- and downscaling opportunities, are not yet well understood.

In this work we report the first experimental fabrication of superfine (sub-100 nm) transverse surface nanoripples on an optically polished surface of a 1.5 mm thick disk-like titanium (Ti, hcp α-phase) sample, mounted on a three-dimensional motorized, PC-driven micro-stage, by multiple, normally incident and weakly focused (1/e-diameter $\approx$1.4 mm) pulses of 744 nm, 110 fs Ti:sapphire laser, running at a repetition rate of 10 Hz [21]. Laser pulse energies, starting from 5 mJ, were varied and monitored by means of a reflective polarizing attenuator and a pyroelectric energy meter (OPHIR), respectively. Local, spatially periodical nanostructuring of the Ti surface (figure 1) was performed at peak (in the center of the laser spot with a Gaussian fluence distribution) laser fluences F with the particular values $F_1 \approx$ 18 mJ cm^{-2} ($N_1 \approx 7 \times 10^2$) and $F_2 \approx$ 14 mJ cm^{-2} ($N_2 \approx$ 2.5×10^4), which are both well below the uniform single-shot melting and ablation thresholds of titanium, $F_{melt} \approx$ 50 and
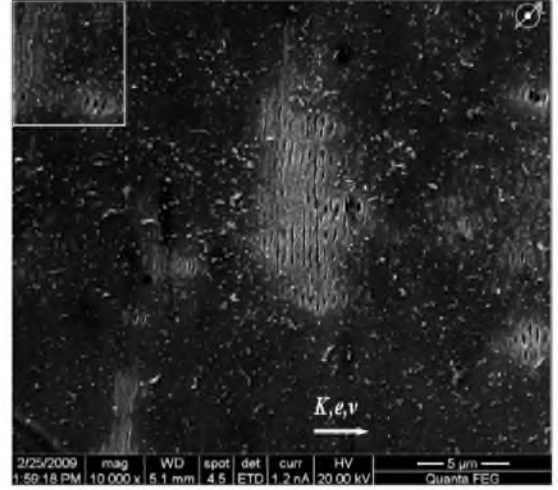
Figure 1. General view SEM image ($\times 10\,000$) of the Ti surface with the central region fs-laser nanostructured at $F_1 \approx$ 18 mJ cm^{-2} and $N_1 \approx 7 \times 10^2$, consisting of periodic longitudinal trenches ($\boldsymbol{K} \parallel \boldsymbol{e}$). Another spot of interest in the left upper corner is highlighted by the white square frame.

$F_{abl} \approx$ 300 mJ cm^{-2} [24], respectively. The nanostructured spots were characterized by means of an SEM (Quanta FEG 600) with a spatial resolution up to 250 000$\times$.

2. Experimental results and discussion

Ti nanostructures fabricated for $F_1 \approx$ 18 mJ cm^{-2} and the number of shots per spot $N_1 \approx 7 \times 10^2$ demonstrate a set of well-defined quasi-periodical sub-micron trenches (the average period $\Lambda_{nano} \approx$ 500 nm) with their wavevectors $\boldsymbol{K}$ ($|\boldsymbol{K}| = 1/\Lambda$) collinear to the polarization $\boldsymbol{e}$ and scanning velocity $\boldsymbol{v}$ (figure 1). The orientation of the trenches ($\boldsymbol{K} \parallel \boldsymbol{e}$) is consistent with the standard 'interference' model of their fabrication via constructive interference between the incident fs-laser and excited SPP wave [10–13]. The trenches, rather than nearly harmonic ripples with the same period, appear because of the moderate laser fluence $F_1 \approx$ 18 mJ cm^{-2}, which is equal to the nanostructuring threshold, $F_{nano} \approx$ 18 mJ cm^{-2} [16]. This becomes clearer at lower fluences $F <$ 18 mJ cm^{-2}, at the periphery of another laser spot (figure 2), where quasi-periodic, longitudinal ($\boldsymbol{K} \parallel \boldsymbol{e}$) surface modification stripes emerge either with or without the axial trenches, or with short or broken ones.

According to their pronounced longitudinal polarization ($\boldsymbol{K} \parallel \boldsymbol{e}$), the above-mentioned surface stripes with the modified material surface with or without trenches appear near to maxima of the 'laser–SPP' interference pattern on the surface, described by the formula for the spatially modulated total fluence F_Σ [13]

$$F_\Sigma(x) = F(x) + (FF_{SPP})^{1/2} \sin\left(\frac{2\pi}{\Lambda_{SPP}}x + \phi\right), \quad (1)$$

where x is the specific spatial coordinate ($\boldsymbol{x} \parallel \boldsymbol{e}, \boldsymbol{v}$), $F(x)$ is the Gaussian distribution of the incident laser fluence, F_{SPP} is the fluence contributed by the SPP wave, and ϕ is some phase shift value. According to this formula,
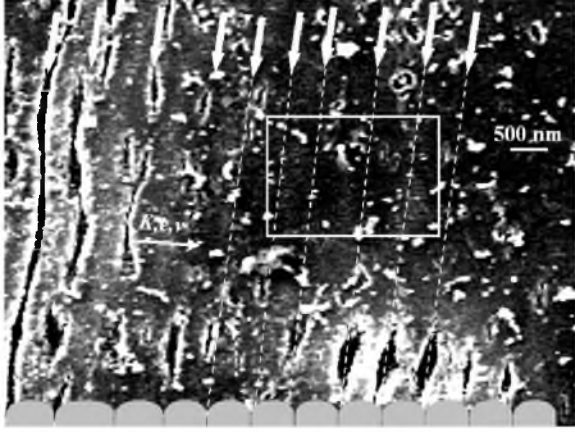
Figure 2. Enlarged SEM view ($\times 50\,000$) of the surface spot highlighted in figure 2, at the periphery of the fs-laser nanostructured region. The vertical arrows show the periodic longitudinal ($K \parallel e$) surface modification stripes with their axial longitudinal trenches, indicated where necessary by the dashed lines. The gray bottom modulated region exhibits schematically the one-dimensional 'laser–SPP interference' surface pattern, corresponding to the spatial profile of the deposited laser energy. The rectangular frame shows the surface region with the stripes nanomodulated in the transverse direction.

the experimentally observed surface stripes with or without axial trenches represent the surface modification regions close to the interference maxima (figure 2), while the axial trenches appear when the peak values $F_\Sigma \geq F_{abl} \approx 0.3$ J cm^{-2} [24]. The last inequality is satisfied for $F_1 \approx 18$ mJ cm^{-2} when, according to equation (1), F_{SPP} approaches ~ 5 J cm^{-2} with the surface electromagnetic (SPP) field concentrated thus by $\sim 10^2$ times because of the diffractive and interference redistribution of the incident plane laser wave into the propagating SPP wave localized within the extremely narrow (compared to the laser spot) near-interface skin layer [12]. Then, at higher fluences F resulting in $F_\Sigma > F_{abl}$, much broader trenches appear in the interference maxima, eventually—for higher F or N—transforming into quasi-harmonic one-dimensional sub-micron nanogratings [15, 16].

Surprisingly, for even farther regions of the laser spot, the longitudinal stripes comprise not the longitudinal (axial) trenches, but much finer transverse ($k \perp e$) nanoripples with periods λ_{nano1} down to 60 nm (figure 3, left inset). More detailed topological analysis via one- or two-dimensional fast Fourier transform (FFT) procedures shows a distinct 1D-orientation of the nanoripples in the presence of the only spatial harmonic with $|k| = 1/\lambda_{nano1} \approx 0.017$ nm^{-1} (figure 3, right inset). This pronounced transverse orientation of the fine nanoripples, perpendicular to the laser polarization e and the wavevector K of the coarse stripes (trenches), at their obvious localization within the longitudinal surface modification stripes, indicates no direct relation (coupling) to the incident laser or SPP wave, but is just mediated by those two through their energy deposition into the material. These brighter lateral surface modification stripes observed in figures 2, 3 show higher charging of these local regions, which may be related to their lower electrical conductivity resulting, potentially, from their perturbed topographic or crystallographic structures.

Moreover, for even more peripheral stripes of the modified Ti surface there are no such transverse nanoripples appearing on them, demonstrating their threshold-like appearance.

An additional experimental observation of such transverse surface nanoripples is provided by SEM images of the Ti surface irradiated by the much larger number ($N_2 \approx 2.5 \times 10^4$ shots/spot) of fs-laser pulses at the laser fluence $F_2 \approx 14$ mJ cm^{-2}, i.e. even below the nanostructuring threshold $F_{nano} \approx 18$ mJ cm^{-2} [16]. The cumulative laser-induced surface damage resulting in this case from multi-thousand thermomechanical loading/unloading cycles takes the form of fatigue-mediated spallation of nanometer-thick, micron-wide metal sheets (figure 4(a)), while the sheets exhibit no periodical and oriented (laser polarization-sensitive) sub-micron damage traces, e.g. longitudinal surface modification stripes and trenches. Indeed, our estimates provide the peak volume energy density $\varepsilon \approx (1-R^*_{744})\alpha^*_{744}F_2 V_M \approx 25$ kJ mol^{-1}, where at $F_2 \approx 14$ mJ cm^{-2} the transient 744 nm Ti reflectivity $R^*_{744} \approx 0.5$ (for the p-polarization and incidence angle of $20°$) and absorption coefficient $\alpha^*_{744} \approx 3.3 \times 10^5$ cm^{-1} [16], and its molar volume $V_M \approx 10.5$ cm^{-3} mol^{-1}. This value is considerably lower than the melt enthalpy ≈ 55 kJ mol^{-1} at the Ti melting temperature $T_{melt} \approx 1603$ °C [25], which can be achieved at the uniform single-shot melting threshold $F_{melt} \approx 50$ mJ cm^{-2} [24]. However, in contrast, these sheets again demonstrate pronounced, harmonic transverse surface modulations (figure 4(b)) with a single spatial period $\lambda_{nano2} \approx 50$–60 nm (figures 4(c), (d)), consistent, within the experimental error bars, to the period λ_{nano1} of the previously observed transverse nanoripples (figure 3).

Importantly, the superfine transverse nanoripples observed in this work for Ti have periods of 50–60 nm, which are almost three–four times lower, than those (≈ 200 nm) of similar transverse nanoripples observed earlier on Al surfaces [21], for quite similar widths of surface stripes occupied by them (≈ 200 nm for Ti in figures 3, 4 versus ≈ 300 nm for Al in [21]). This may mean that such sub-micron stripe widths have a minor effect on $\lambda_{nano1,2}$ in terms of transient stress localization yielding in local surface distortions, compared for example to the much higher high-temperature heat conductivity Θ of molten l-Al (93 versus 20 W m^{-1} K^{-1} even for solid s-Ti at 1000 °C [26]), its lower surface tension σ (915 mN m^{-1} for l-Al at 660 °C [26] versus 1557 mN m^{-1} for l-Ti at the melting temperature of 1608 °C [27]), and its lower viscosity η (1.5–2 mPa s for l-Al at 730 °C [26] versus 4.4 mPa s for l-Ti at 1608 °C [27]). Indeed, generally, cavitation dynamics is driven by a number of diverse factors, e.g. tension, inertia, and viscosity [28]

$$P' = P_S + \frac{4\sigma}{D} + \frac{\rho D}{4}\left(d^2D/dt^2\right) + \frac{3\rho}{4}(dD/dt)^2$$
$$+ \frac{4\eta}{D}(dD/dt), \qquad (2)$$

where D is the bubble size, P_S is the equilibrium vapor pressure, and ρ is the melt density. Specifically for fs-laser driven cavitation in surface melts of GaAs and Si [21, 29], it occurs as a quasi-equilibrium sub-surface nanoscale process on the characteristic temporal and spatial scales $\tau \sim$
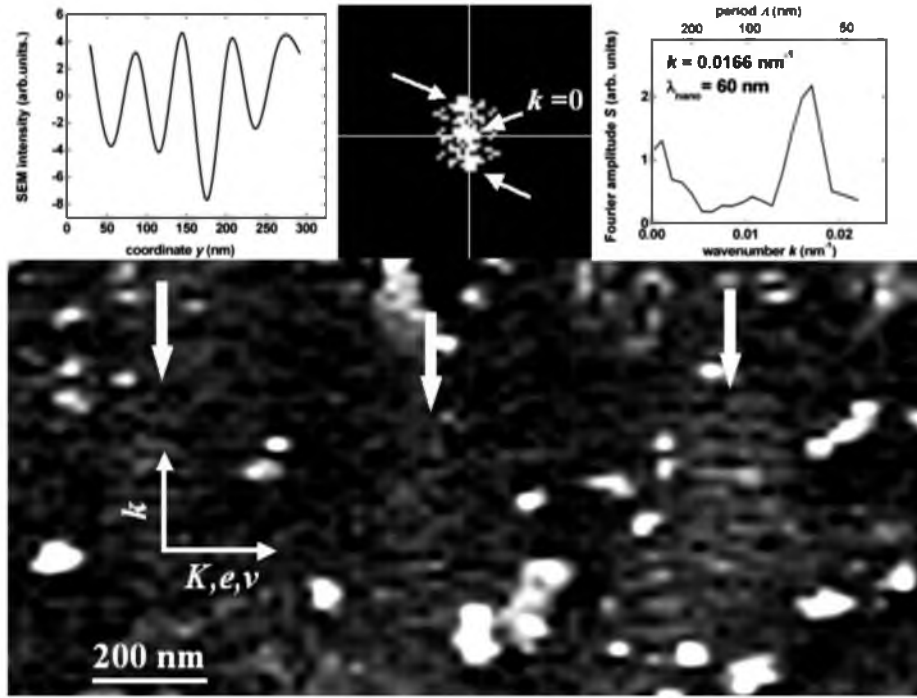
Figure 3. Enlarged SEM view (200 000×) of the region highlighted by the rectangular frame in figure 3, at the farther periphery of the fs-laser nanostructured region. The vertical arrows show the light periodic longitudinal surface modification stripes ($K \parallel e$), containing their transverse ($k \perp e$) nanoripples. The left, central and right insets show the surface relief profile, its two- and one-dimensional FFT spectra, respectively, with the arrows in the two-dimensional FFT spectrum (central inset) indicating the zero (crossing) point $k = 0$ and the symmetrical reflexes of the transverse nanograting.
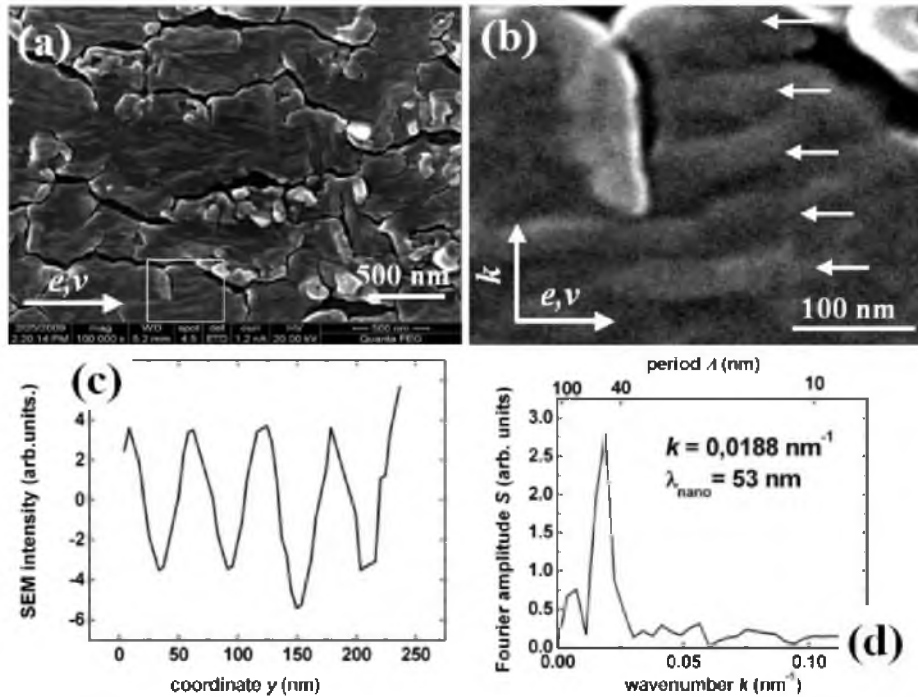
Figure 4. (a) General SEM view of the Ti surface fs-laser nanostructured at $F_2 \approx 14$ mJ cm^{-2} and $N_2 \approx 2.5 \times 10^4$, with the spot of interest highlighted by the rectangular white frame. (b) The enlarged SEM view of the spot in (a) exhibiting the periodical transverse ($k \perp e$) modulation (nanoripples) shown by the short horizontal arrows. (c) The relief profile of the transverse surface modulation in (b) within the circle. (d) FFT spectrum of the transverse surface modulation in (c).

10^2–10^3 ps and $D \sim 10^1$–10^2 nm, respectively, in acoustically relaxed melts of these materials. Under such conditions, one can derive a phenomenological scaling relationship for D as a function of the main thermal variables Θ and σ

$$D \propto \frac{\sqrt{\Theta}}{\sigma}, \tag{3}$$

where D represents the dimensions of super-critical 'frozen' nanobubbles, rather than their critical size [28, 30]. The factor in the numerator tends to extend nanocavitation-related heat transport to longer spatial scales, while the factor in the denominator reflects the melt resistance to cavitation owing to the quasi-static surface tension effect (the kinetic viscosity effect represented by the last term in equation (2) can be neglected under these quasi-equilibrium cavitation conditions) [28, 30]. As a result, the estimates of D for Al and Ti melts taken according to equation (3) for the above-mentioned values of Θ and σ, exhibit a ratio $D_{Al}/D_{Ti} \approx$ 3–3.5 in good quantitative agreement with the experimental values of their superfine transverse nanoripple periods given above. In contrast, if the dynamic viscosity effect is taken into account, making the cavitation process even more non-equilibrium, this ratio D_{Al}/D_{Ti}, owing to the appearance of the factor η in the denominator to provide dynamic viscous resistance to the nanobubble formation, increases to the much less reasonable magnitude of 6–7.

In conclusion, we have for the first time observed sub-100 nm transverse nanoripples appearing on titanium surfaces under multi-shot sub-threshold fs-laser irradiation. Surprisingly, these transverse nanoripples emerge exactly along the maxima of the fs-laser–SPP interference surface pattern visualized by SEM in the form of a quasi-periodical surface grating of longitudinal surface modification stripes, with its wavevector collinear to the laser polarization. According to previous MD simulations and our brief analysis, these sub-100 nm nanoripple structures can be related to frozen patterns of coherent sub-surface nanoscale cavitation (among other possible nanostructuring mechanisms), providing new opportunities for surface nano-engineering on a sub-100 nm scale.

Acknowledgments

References

[1] Borowiec A and Haugen H K 2003 *Appl. Phys. Lett.* **82** 4462–4

[2] Wu Q, Ma Y, Fang R, Liao Y, Yu Q, Chen X and Wang K 2003 *Appl. Phys. Lett.* **82** 1703–5

[3] Bonse J, Munz M and Sturm H 2005 *J. Appl. Phys.* **97** 013538

[4] Zhao Q Z, Ciobanu F and Wang L J 2009 *J. Appl. Phys.* **105** 083103

[5] Shen M Y, Crouch C H, Carey J E and Mazur E 2004 *Appl. Phys. Lett.* **85** 5694–6

[6] Carey J E, Crouch C H, Shen M Y and Mazur E 2005 *Opt. Lett.* **30** 1773–5

[7] Vorobyev A Y, Makin V S and Guo C 2009 *Phys. Rev. Lett.* **102** 234301

[8] Baldacchini T, Carey J E, Zhou M and Mazur E 2006 *Langmuir* **22** 4917–9

[9] Vorobyev A Y and Guo C 2010 *Opt. Express* **18** 6455–60

[10] Sipe J E, Young J F, Preston J S and van Driel H M 1983 *Phys. Rev.* B **27** 1141–54

[11] Akhmanov S A, Emel'yanov V I, Koroteev N I and Seminogov V N 1985 *Usp. Fiz. Nauk* **147** 675–745
Akhmanov S A, Emel'yanov V I, Koroteev N I and Seminogov V N 1985 *Sov. Phys.—Usp.* **28** 1084–124 (Engl. transl.)

[12] Klimov V V 2009 *Nanoplasmonics* (Moscow: Fizmatlit) (in Russian)
See also Raether H 1988 *Surface Plasmons on Smooth and Rough Surfaces and on Gratings* (Berlin: Springer)

[13] Makin V S, Pestov Yu I, Makin R S and Vorob'ev A Ya 2009 *J. Opt. Technol.* **76** 555–9

[14] Sakabe S, Hashida M, Tokita S, Namba S and Okamuro K 2009 *Phys. Rev.* B **79** 033409

[15] Golosov E V, Emel'yanov V I, Ionin A A, Kolobov Yu R, Kudryashov S I, Ligachev A E, Novoselov Yu N, Seleznev L V and Sinitsyn D V 2009 *JETP Lett.* **90** 107–11

[16] Golosov E V, Ionin A A, Kolobov Yu R, Kudryashov S I, Ligachev A E, Novoselov Yu N, Seleznev L V and Sinitsyn D V 2011 *JETP* **113** 14–26

[17] Golosov E V, Ionin A A, Kolobov Yu R, Kudryashov S I, Ligachev A E, Makarov S V, Novoselov Yu N, Seleznev L V, Sinitsyn D V and Sharipov A R 2011 *Phys. Rev.* B **83** 115426

[18] Inogamov N A *et al* 2010 *Appl. Phys.* A **101** 87–96

[19] Bashir S, Rafique M S and Husinsky W 2009 *Appl. Surf. Sci.* **255** 8372–6
Rafique M S, Bashir S, Husinsky W, Hobro A and Lendl B 2012 *Appl. Surf. Sci.* **258** 3178–83

[20] Ishino M *et al* 2011 *J. Appl. Phys.* **109** 013504

[21] Ionin A A, Kudryashov S I, Ligachev A E, Makarov S V, Seleznev L V and Sinitsyn D V 2011 *JETP Lett.* **94** 266–9

[22] Zhakhovskii V V, Inogamov N A and Nishihara K 2008 *JETP Lett.* **87** 423–7

[23] Ionin A A, Kudryashov S I, Seleznev L V and Sinitsyn D V 2011 *JETP Lett.* **94** 753–8

[24] Ye M and Grigoropoulos C P 2001 *J. Appl. Phys.* **89** 5183

[25] Grigor'ev I S and Meylikhov E Z 1991 *Physical Quantities* (Moscow: Energoatomizdat)

[26] Alfe D and Gillan M J 1998 *Phys. Rev. Lett.* **81** 5161–4

[27] Paradis P F, Ishikawa T and Yoda S 2002 *Int. J. Thermophys.* **23** 825–42

[28] Debenedetti P G 1996 *Metastable Liquids: Concepts and Principles* (Princeton: Princeton University Press)

[29] Ionin A A, Kudryashov S I, Seleznev L V, Sinitsyn D V, Bunkin A F, Lednev V N and Pershin S M 2013 *JETP* **143** 347–62

[30] Skripov V P, Sinitsyn E N, Pavlov P A, Ermakov G V, Muratov G N, Bulanov N V and Baidakov V G 1988 *Thermophysical Properties of Liquids in the Metastable (Superheated) State* (New York: Gordon and Breach)

[31] Ionin A A, Golosov E V, Kolobov Yu R, Kudryashov S I, Ligachev A E, Makarov S V, Seleznev L V and Sinitsyn D V 2012 *AIP Conf. Proc.* **1464** 386–96

[32] Bonse J, Höhm S, Rosenfeld A and Krüger J 2013 *Appl. Phys.* A **110** 547–51